Systematic evaluation of a microwave medical imaging system

Matilde P. Moreira, nº84137, IST, Carlos A. Fernandes, IST, and João M. Felício, IST

Instituto Superior Técnico, Av. Rovisco Pais 1, 1049-001, Lisbon, Portugal

Instituto de Telecomunicações, Lisbon

matildemoreira@tecnico.ulisboa.pt

Abstract—The breast cancer has the highest cancer attack-rate among women. The standard methods of breast cancer detection are painful, time consuming, expensive and harmful. The drawbacks of these methods have resulted in research into alternative methods of breast imaging. Microwave Breast Imaging (MWI) has received attention for many years. The Antennas and Propagation group at Instituto de Telecomunicações has been working in medical imaging techniques based on microwave radar and they developed a contactless microwave imaging system, that is a dry setup, for breast cancer screening. A Graphical User Interface is used to control the system along with adequate signal processing. In this dissertation, it is also possible to know the changes in the interface and the setup. In order to deal with the challenges of the dry setup exists an algorithm based on singular value decomposition (SVD), that removes the skin back-scattering. There exist two calibration methods to remove the early time reflections: the Ideal Calibration and the SVD. Before submitting the setup to clinical trials, it is important to test the set-up in controlled environment using phantoms. This dissertation demonstrates the results of the test using a set of breast phantoms anthropomorphic. The numerical results include the study of the behavior of the XETS antenna depending on distance to the target, in order to understand how the distance of the XETS antenna affects the results during the experimental measurements with breast phantoms. The results were promising, as it was possible to detect the tumors for most breast phantoms.

Index Terms—breast cancer, microwave imaging (MWI), artifact removal, phantom, measurement setup

I. INTRODUCTION

GLOBAL statistics indicate that breast cancer is the most frequently diagnosed invasive cancer and the second cause of death by cancer among female patients.[1], [2] Technology has had a strong impact on the early detection of cancer, through improved treatment methods, the implementation of screening programs and improved imaging techniques.[3], [4] Nowadays, the current conventional imaging applications used in breast cancer detection are X-Ray mammography, Magnetic Resonance Imaging (MRI) and ultrasound.[4]

Mammography exposes the patient to ionizing radiation and is very painful to the patient.[5]. Magnetic Resonance Imaging (MRI) is non-invasive technique, which uses strong magnetic fields to produce high resolution and quality of images of the breast, but is expensive, time-consuming, claustrophobic and is also contraindicated in patients having pacemakers and other type of implants.[6] Ultrasound is a non-ionizing, painless, low cost, but shows small resolution, is time consuming and the examiner influences effectiveness of the results and the

"sonogram" obtained. [3], [7] All these modalities exploit a variety of properties of biological tissues to form an image, whose aspects are summarized in the Table I.

TABLE I: Comparisons between different imaging techniques for breast cancer detection [8].

Imaging Techniques	Patients Comfort	Radiation Safety	Cost	Time Required
X-ray mammography	Uncomfortable	Ionizing Radiation	Low	Less than 10min
Ultrasound	Comfortable	Non-ionizing Radiation	Low	15-25 min
MRI	Uncomfortable	Non-ionizing Radiation	High	45min-1hr

In order to overcome the shortfalls of the aforementioned screening methods, Microwave Breast Imaging (MWI), a low cost and non-ionizing imaging modality that represents a promising imaging modality of breast cancer detection, is being investigated. MWI exploits the contrast of dielectric properties of biological tissues to form images, potentially providing complementary information to conventional diagnoses. [16], [3], [4], [5], [1] For all the reasons presented, MWI is an ideal candidate for large scale screening campaigns and post-treatment cancer surveillance.[17] It is common to categorize active MWI as Tomography and Ultra wide-Band (UWB) radar. The tomographic approaches aim to reconstruct the dielectric breast profile based on dielectric properties, using non-linear inversion algorithms.[9], [17] Alternatively, the radar approach belongs to the class of linear scattering techniques, which is much faster computational signal processing.

Several operational microwave systems have been employed to trials to investigate the clinical feasibility of MWI. [4] The Table II shows the differences between the operational microwave systems in terms of technical design parameters, patient interface and reconstructions algorithms.[4]

By analysis of Table II, most operational systems require the patient to lie prone on an examination table, but there are also systems that require the breast to be immersed in a coupling medium or to be in direct contact with a solid coupling shell. Regarding the technical design, most operation systems collect multi static data, where it is used different antennas to record and transmit, but monostatic acquisition has been also investigated, where the same antenna transmits and records the reflected signals. The challenges that imaging operating systems and clinical evaluations face are related to

TABLE II: Summary of microwave breast imaging systems developed. [6]

Systems	Largest trial	Position	Imaging	Freq [GHz]	Antenna	Scan Time	Acquisition
MARIA,UK [6]	223	prone	Radar	3-8	slot	10s	frequency
DC,USA [9]	150	prone	Tomo	0.7-1.7	monopole	5min	frequency
MU (Table) [4]	13	prone	Radar	2-4	TWTLTLA	18min	time
MU (wearable) [4]	38	seated	Radar	2–4	microstrip	5min	time
SUST, China [4]	11	prone	Radar	4–8	horn	4min	frequency
TSAR, Canada [6], [4]	8	prone	Radar	1.3–7.6	vivaldi	30min	frequency
HU, Japan [9]	5	supine	Radar	3.1–10.6	planar slot	3min	time
SU, Japan [10]	2	prone	Radar,Tomo	4–9	stacked patch	3min	frequency
Microwave Vision [11]	pilot	prone	Radar	1–4	vivaldi	10min	frequency
Mammowave, Italy [12], [6]	51	prone	HP	1–9	PulsON P200	10min	frequency
Kobe University, Japan [6]	20	supine	Tomo	0.05–12	UWB	30min	time
ETRI, Korea [6], [13]	15	prone	Tomo	3–6	monopole	15 s/slice	frequency
Manitoba, Canada [14], [15]	-	prone	Radar,Holo	1–8	horn	-	frequency

the influence of the technical design parameters on clinical use, the effect of the acquisition hardware and algorithm design on the patient scan time and the system mechanical complexity and the implications for design safety.

In recent years, the Antennas and Propagation group of Instituto de Telecomunicações (IT), at Instituto Superior Técnico, in Lisbon, has been working and acquired experience in medical imaging techniques based on microwave radar (MWI). This experience has been acquired through the development of a contactless microwave imaging system for breast cancer screening to be submitted to clinical trials. The group has already developed an application with user friendly interface to control the system along with adequate signal processing algorithms to cope with the inherent challenges that MWI faces.

Prior to clinical trials, it is important to test the set-ups in controlled environment through the use of phantoms.

The phantoms are an artificial structure that mimics the properties of the human body, such as the electric properties, light scattering and optics and sound wave reception. [18] There are three types of primary phantoms used in the literature: solid, liquid and gel phantoms. The phantoms are normally hollow and carry a prepared solution according to a recipe, although the liquid phantoms degrade with time. Gel phantoms must be individually prepared by hand and are therefore unique, although the material can closely model the dielectric properties of breast tissues. [19] Solid phantoms use solid materials as the tissue mimicking materials and they are robust, stable and can be 3D-printed, allowing its replication. One of limitations of this type of phantom is due to its unique geometric shape and the fact that it cannot be modified because the components are solid. [20]

Within this framework the goals of this master's dissertation are:

- Use the IT MWI set-up to examine a set of phantoms developed at a Manitoba university that collaborates with IT;
- Develop the MWI image acquisition set-up of IT, to prepare it for the clinical tests stage in hospitals;
- Further develop the Graphical User Interface (GUI), which interacts directly with the user and operates the setup. A part of the interface was developed in previous works. [21], [22]

- Improve the IT set-up and methods of reconstructing the medical image of the breast from radar echoes.
- Implement calculation acceleration strategies to allow obtaining images of the breast in real time.

II. FORMULATION

A. Migration Algorithm

The presented radar-based method in this section, whose name is Matched Filter, is based on wave migration, which "back-propagates" the wave-front.The migration algorithm accounts for the phase-delay of the propagating wave.[21], [22]

In order to find where the target is located, the imaging algorithm considers a "search" volume, which contains the target, as shown in Figure 1.
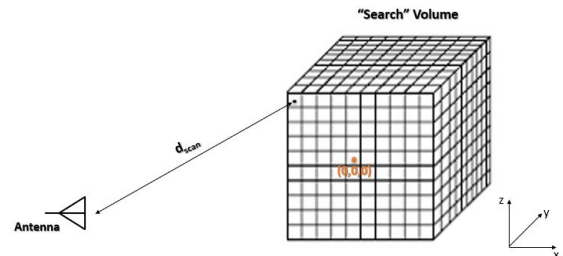

Fig. 1: "Search" volume containing the target. Each focal point scatters the signals transmitted by the antenna.

In order to guarantee that the algorithm processes uniquely the scattered signal from target, it is necessary the realization of a calibration procedure. The calibration procedure is the ideal, subtracting the reflection coefficients from the configuration with the target and the reflection coefficients from the scenario without the target according to Equation 1

$$S_{11final(i,j)} = S_{11data(i,j)} - S_{11calibration(i,j)} \qquad (1)$$

where $S_{11data(i,j)}$ and $S_{11calibration(i,j)}$ are data obtained and (i,j) is the index of the antenna position.

The migration algorithm tests each focal point individually and if the distance of the scan point to the antenna,d_{scan}, matches the distance of the target,d_{target}, it is possible to cancel the phase of the reflected wave. In order to obtain a detection of the target, the algorithm consists in, for every

point of the "search" volume, multiplying the phase of the reflected wave by the frequency dependent S-parameters, for each position of the antenna, as shown in Equation 2.

$$Image = \sum_r |\sum_{i,j} S_{11final(i,j)} \times e^{2jk_r(d_{scan(i,j)}+d_{ant})}| \quad (2)$$

where r is the index of frequencies, s11 is complex, n is the index of refraction of the respective medium, (i,j) is the index of the antenna position and d_{ant} is the electrical distance of the antenna.

B. Artifact Removal Algorithm

Since the value of permittivity contrast between skin and air is high, the received signals are dominated by this early-time reflection. The artifact is larger in magnitude than the tumor response, which can mask the tumor and prevent its detection. In order to avoid this, it is necessary to remove or at least reduce the early-time response from the skin. This processing step is known as artifact removal. The algorithm developed in order to use a dry setup is the Singular Value Decomposition (SVD), a fast and real-time artifact removal algorithm used in the calibration, which decomposes the measured data into a set of reflections, allowing removing the stronger echoes created by the breast skin, without influencing the tumor position, as can be seen in greater detail in [23], [21] and [22].

Figure 2 represents a propagation scenario considering a antenna *a* and one neighbour antenna, *a-N1,a+N1*, on each side of the selected antenna,*a*. d_s^{init} corresponds to the shortest distance between the antenna and the breast skin,d_t, the distance from the skin to the tumor and d_s^{back}, the physical distance between opposite walls of the breast. Ts corresponds to the transmission coefficient of the skin and $\Gamma_s^{init},\Gamma_s^{back}$ and Γ_t are the reflection coefficients of the front skin interface, opposite skin interface, and tumor, respectively.

In order to ensure that the unwanted antenna internal reflections are removed from the scattered signals, the signal processing considers that the signals retrieved in the presence of the breast are subtracted by the free-space antenna input reflection coefficient.
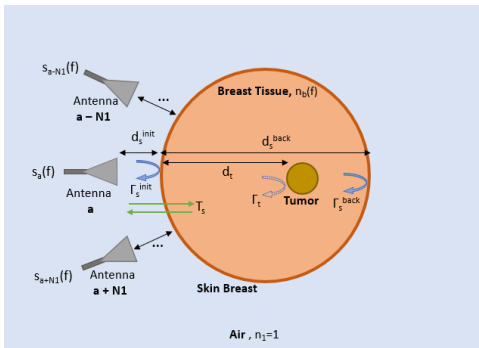

Fig. 2: Sketch of the antenna symmetry and a simplified propagation scenario for one antenna and its neighbours.

The Equation 3 represents the calibration matrix, S_a^{cal} (i.e. without the skin artifact) is obtained by subtracting the matrix

for the input reflection coefficients for the selected antennas, according to the number of neighbors defined, by the optimal approximation matrix of SVD, M_q, where q represents the singular values.

$$S_a^{cal} = S_a - M_q \quad (3)$$

The value of q is obtained by applying the inverse discrete Fourier transform (IDFT) to the time signals of matrix S_a^{cal} and the maximum value of q is defined until the reflected signal is out of the breast.

C. Image Quality Metrics

In order to quantitatively analyze the images reconstructed from the processing of measurements acquired using the phantoms anthropomorphic, three image performance metrics were used, namely the Positioning Error(PE),Tumor-to-clutter Ratio (TCR) and Tumor-to-mean Ratio(TMR) to assess the quality of the received signals and the image reconstruction, as seen in the table III. [16]

In log units, TCR and TMR are computed as presented in equations 4 and 5, respectively. The TCR and TMR provide a measure of the contrast between the clutter and the tumor responses in the reconstructed images.[24]

$$TCR[dB] = 10log_{10}[max(T)/max(C)] \quad (4)$$

$$TMR[dB] = 10log_{10}[max(T)/mean(C)] \quad (5)$$

The Positioning Error is defined in equation 6

$$PE = ||P_{tumor} - P_{detected}|| \quad (6)$$

where P_{tumor} is the known tumor position and $P_{detected}$ is the position of the maximum response in the reconstructed image.

III. DESIGN AND SIMULATION RESULTS

This chapter addresses the numerical results of the study of the behavior of the Crossed Exponentially Tapered Slot (XETS), ultrawideband antenna, [25], depending on distance to the target. The XETS antenna is used in the measurement of signals acquired with different phantoms anthropomorphic and which is presented in the next section, that is section IV.

A. Design Description

During the experimental analysis, different breasts phantoms anthropomorphic were measured using a VNA. The breasts differ in shape and dimensions, with, for example, some breasts being more elliptical than others. After obtaining the dispersion data, it was found that despite the ideal calibration method perfectly detecting the tumor, the SVD algorithm did not detect the same in some breasts, namely large and/or elliptical breasts.

In order to understand the impact of the distance from the antenna to the breast skin on the results obtained, we resorted to the Computer Simulation Technology (CST) Microwave

TABLE III: Performance metrics used to assess the qualify of the received signals and the image reconstruction [16].

Performance Metrics	Description
Tumor response magnitude,T	Measure the intensity of the tumor response in the final image.
TCR	Measure T relative to the largest intensities of the background clutter of the image,C
TMR	Measure T relative to the mean intensities of C.
PE	Quantify the deviation of the detected tumor relative to the actual coordinates.

Studio. [26] The antenna used is the XETS antenna and since it works between 2.4 GHz and 4.8 GHz [27], the frequency interval considered was between 2 and 5 GHz.

In the CST, a setup was developed consisting of the antenna used in the laboratory, XETS, and a rectangular parallelepiped metal target, whose dimensions are $160 \times 160 \times 2mm^3$, as shown in Figure 3. The XETS antenna is 5mm away from the metal target.
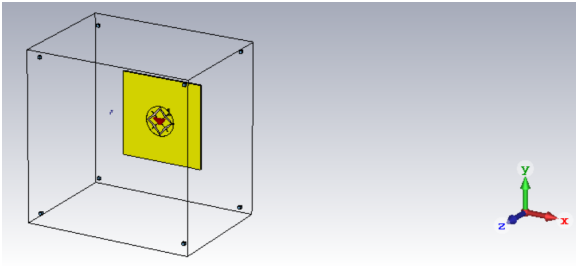

Fig. 3: Perspective View of XETS antenna and metallic target.

As far as the simulations are concerned, two simulations were made, one considering the metallic target and one not considering the target, which corresponds a free space measurement. The material used for the target is copper, as it is an electrical conductor and has an electric conductivity of $5.8 \times 10^7 S/m$.

Through the CST, a linear scan of the position of the antenna in relation to the metallic target was performed between 5mm (initial position of the antenna) and 125 mm (final position of the antenna), every 1 mm, which corresponds to 121 positions of the antenna, in order to obtain the reflection coefficients for each of these positions.

B. Design Results

After obtaining the reflection coefficients for each of the antenna positions and for the two simulations referred in the previous section, the simulation results were analyzed and for this the Matched Filter algorithm was used.

The reflections coefficients for the simulations are subtracted in order to remove the influence of the surrounding environment, since the only difference between the both simulations referred above is the presence of the metallic target.

Through the Matched Filter algorithm, it was possible to visualize the different graphs of the reflected power as a function of the distance for different positions of the antenna in relation to the metallic target. By analyzing the multiple graphs and using computational tools, namely MATLAB, it was possible to determine the different distances for the maximum in the graphs. The maximum value represents the position of the metallic plane.

In Figure 4, it is possible to visualize the relationship between the physical distance from the antenna XETS to the metallic target and the maximum distances discussed above for a frequency of 2 to 5 GHz. It is also possible to visualize in Figure 4, in green, the dotted and straight line resulting from the simple linear regression process, which describes the relationship mentioned above.
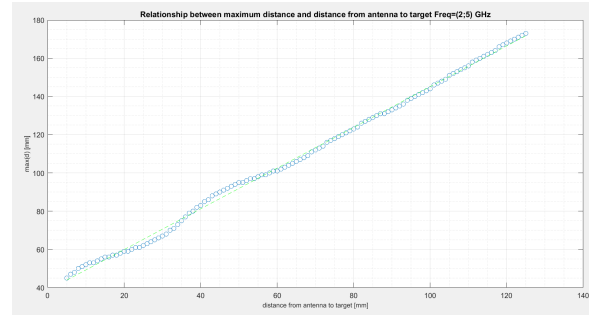

Fig. 4: Relationship between maximum distance and the distance from antenna to the target for a frequency of 2 to 5 GHz.

Analyzing Figure 4, it can be seen that as the XETS antenna moves away from the metallic plate, the values obtained from the relationship tend to approach the simple regression line, reducing the deviation of the points from the line. If the antenna is approached to the metallic target, it is verified that the points obtained present a sinusoidal behavior compared to the simple regression line. In order to understand the deviation of the target's position from its physical position, we proceeded to graph the difference between the different points in Figure 4 in relation to their position in the linear regression line for the frequency band from 2 to 5 GHz, as shown in Figure 5.
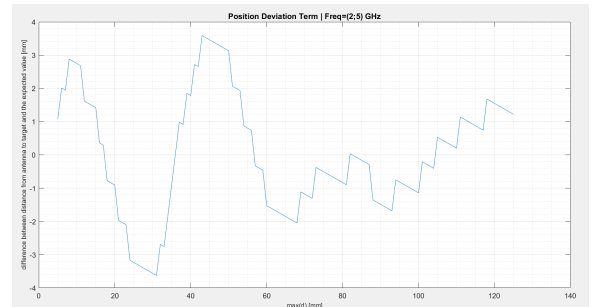

Fig. 5: Position Deviation Term for a frequency of 2 to 5 GHz

By analyzing figure 5, it can be seen that for the 2 to 5 GHz frequency band, the metallic plate can be deviated up

to +- 3.6 mm from its physical position. If we consider the case of the XETS antenna distanced from the breast with the tumor instead of the metallic plane, the result obtained in figure 5 reflects the situation that when using the algorithm to reconstruct the image of the breast with the tumor, the breast skin may appear in the image shifted from its original position, which leads to the tumor also being deviated.

Through the analysis of the Figure 5, it can be seen that the deviation from the target position decreases as the antenna moves away from the metallic target and the behavior of the graph may be related to the presence of a standing wave, formed by the superposition of two identical waves, but in opposite directions, derived from the metal plate that reflects the signal to the XETS antenna again.

IV. EXPERIMENTAL RESULTS

This section covers the two topics: experimental results of some set of phantoms anthropomorphic and homogeneous and the further development of the microwave image setup, as it is divided into two sections.

In the first section, different sets of phantoms anthropomorphic are measured and image reconstruction of these phantoms using the IT MWI reconstruction algorithm.

Regarding the second section, it consists of the description of the MWI IT image acquisition setup, as well as the development of an user-friendly graphical user interface that in turn interacts directly with the user and operates the configuration, which creates a bridge between the setup and the technicians and doctors to perform the examination. It is noteworthy that some part of the interface has already been developed in previous works.[21], [22]

A. Measurement of Signal acquired using phantoms anthropomorphic

The breast phantoms were experimentally measured using an Agilent E5071C vector network analyzer.

The image reconstruction algorithm used to reconstruct all the images presented in this section uses a 5mm distance between pixels and an average dielectric permittivity for the phantom of 4.2.

1) Hagness Breast: The first experimentally measured breast phantom was the Hagness, that is a 3-D-printed Polyactic acid (PLA) shell ($\varepsilon_r \approx 2.75 - j0.03$ at 4 GHz), obtained from the University of Wisconsin–Madison breast repository [27].

In figure 6, it is possible to visualize the exterior of the phantom in an xOz plane.

During the experimental analyzes, the Hagness breast phantom was filled with a Triton X-100 surfactant solution, which has a relative permittivity of approximately 4.2 and the tumor containers were filled with a mixture of TX-100, distilled water and sodium chloride of different percentage of each ingredient in order to mimic the dielectric properties of biological tissues. A biologically relevant contrast between the Hagness breast plastic and the solution can be achieved by choosing an appropriate ratio between Triton X-100 and distilled water. [17]
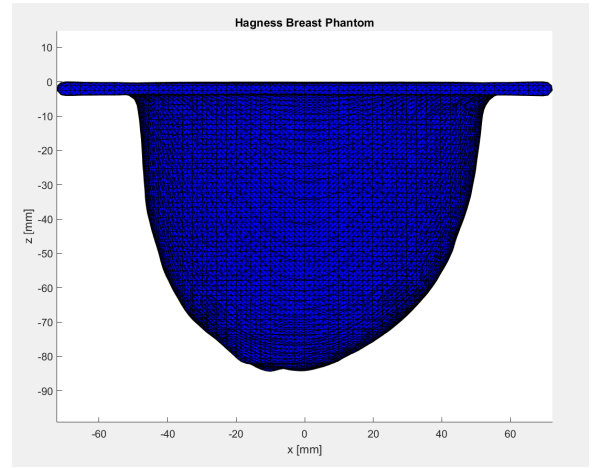

Fig. 6: Representation of the Hagness breast phantom in the xOz plane, that is the anthropomorphic exterior of the phantom.[20]

The Tumor used in the second measurements for the three positions was 3D-printed using conductive Polyactic acid(PLA) filament, usually known as "Proto-pasta", which presents $\varepsilon_r \approx 20 - j9$ at 4 GHz. The "Proto-pasta" has lower dielectric properties compared with a real tumor, but the contrast allows to distinguish it from the fat tissue. [28] Three different tumor position were concerned. The central coordinates of the positions of Tumor used in these measurements are:

- Tumor 1: $(x_t, y_t, z_t) = (20, -15, -43.5)mm$
- Tumor 2: $(x_t, y_t, z_t) = (-20, -5, -43.5)mm$
- Tumor 3: $(x_t, y_t, z_t) = (10, -20, -43.5)mm$

In the experimental measurements with the Hagness breast phantom, the XETS antenna was used. XETS is a thin planar printed antenna and was developed at the Antennas and Propagation Group at Lisbon. The other aspects related with XETS antenna is that its a low-cost, light-weight and low-profile antenna. Furthermore, XETS is the ideal antenna candidate for microwave imaging systems.

In order to obtain the reflection coefficients it was used an Arduino Uno and a motor that allowed rotating the antenna in around the breast, making it easier to obtain measurements.

A linear sweep of the XETS antenna rotation angle between 0º and 360º performed every 9º, instead the 15º, as happened with the previous experimental measurements and analysis with the BAVA antenna. Considering the linear sweep of this second experimental measures, it appears that it corresponds to 40 XETS antenna positions, in order to obtain the reflection coefficients for each of the three tumor positions. It is important to note that the XETS antenna rotates anticlockwise around the Hagness breast.

The figure 7 corresponds to a representation of the 40 XETS antennas around the Hagness breast phantom distanced from the center of the breast (R).

The images that appear below resulted from the application of a reconstruction algorithm and correspond to each tumor position and each calibration method, that is, the ideal cali-

Fig. 7: All 40 XETS antennas around the Hagness breast phantom, where R is the distance between the center of the breast and the position of the antenna.

(a) Ideal Calibration, Tumor 1

(b) SVD, Tumor 1

(c) Ideal Calibration, Tumor 2

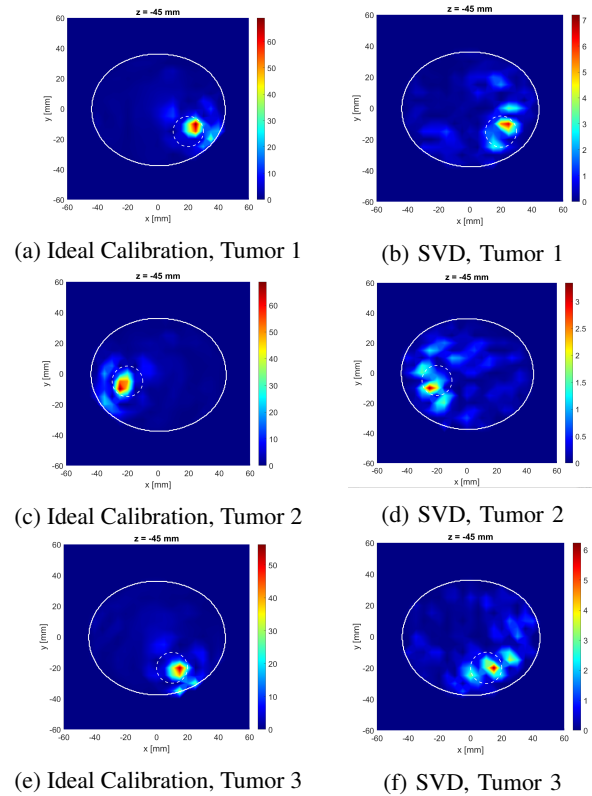(d) SVD, Tumor 2

(e) Ideal Calibration, Tumor 3

(f) SVD, Tumor 3

Fig. 8: Imaging results for the plane z=-45mm considering the three tumors, all XETS antennas and using 8a the ideal calibration 8b the SVD. The white lines translate the border of the breast with the air and the border between the tumor and the fat.

bration method and SVD. The results obtained according to the two calibration methods discussed above for the z = -45 mm plane considering the three tumors for the 40 XETS antennas can be seen in figure 8.

By looking at figure 8a, it is seen that Tumor 1 can be clearly detected using optimal calibration without the presence of any clutter, despite the tumor being deviated from its actual position. Regarding the application of the SVD method, as it is possible to see in figure 8b, it appears that the tumor is detected, with a lower intensity than the ideal calibration, which makes sense, since the ideal calibration removes all interference between measurements with and without tumor. However, there is the presence of clutter close to the tumor.

Subsequently, the images for Tumor 2 were reconstructed according to the two methods mentioned above and the results can be seen in figures 8c and 8d. Using the ideal calibration method and according to figure 8c, the detection of a slightly deviated Tumor 2 is verified. It is possible to detect Tumor 2 using the SVD method with 4 neighbours despite the marked presence of clutter, as it can be seen in figure 8d.

Finally, the figures 8e and 8f represents the results obtained using the Ideal Calibration and SVD method considering the Tumor 3. From the figures 8e and 8f obtained, it appears that Tumor 3 can be equally detected with both methods, despite the presence of clutters in the case of SVD, which can be related with high values of q singular values at SVD that will lead to the decrease of the power of the signal and consequently the tumor answer.

2) A3 Breast: In this subsection, the study of the images obtained by the image reconstruction algorithm for the A3 breast, from the signals measured experimentally with the XETS antenna and with the VNA, is discussed.

Thee A3 breast is a 3-D-printed PLA shell ($\varepsilon_r \approx 2.75 - j0.03$ at 4 GHz).

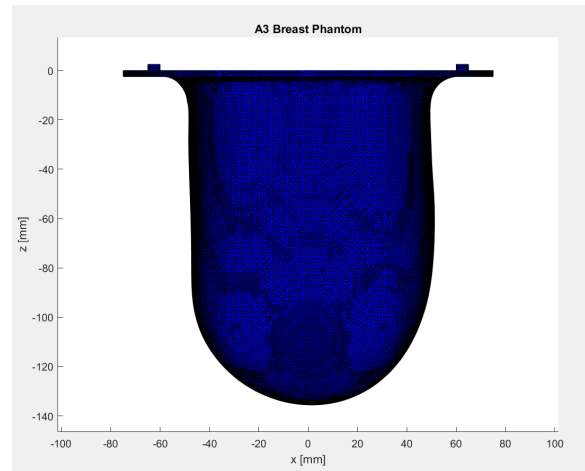Figure 9 represents the outside of the breast in the xOz plane.

Fig. 9: Representation of the A3 breast in the xOz plane.

Figure 9 shows the A3 breast mask is very dense, elliptical and large, which can hinder the process of image reconstruction by using the SVD method.

Before the experimental measurements, the A3 breast was filled with a Triton X-100 surfactant solution of permittivity of $\varepsilon_r \approx 4 - j0.17$ at 4 GHz that mimics the dielectric properties of

biological tissues. Regarding the tumor, its container was filled with a mixture of TX-100, distilled water and sodium chloride with the same dielectric properties of malignant tissues ($\varepsilon_r \approx 55 - j3$ at 4 GHz). The recipes of both liquids are reported in [29].

In order to obtain the measurements of the signals, the XETS antenna position around the A3 breast was scanned, starting at 0º and ending at 360º, with a variation of 15º, which corresponds to 24 possible antenna positions, as it is possible see in figure 10.
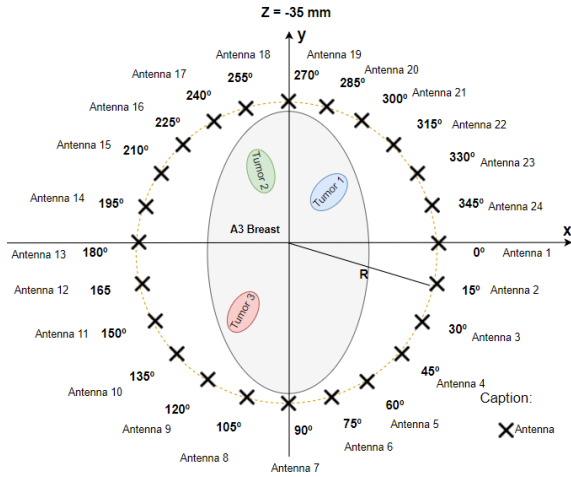
Fig. 10: All 24 XETS antennas around the A3 breast phantom, where R is the distance between the center of the breast and the position of the antenna.

Then, using the image reconstruction algorithm, different images were obtained for the three positions of the tumor, using the ideal calibration method and the SVD calibration method.

The imaging results for the plane z = -35 mm based on experimental data obtained considering the three tumors are shown in figure 11.

The coordinates of the tumors are:
- Tumor 1 $(x_t, y_t, z_t) = (20, 20, -30)mm$
- Tumor 2 $(x_t, y_t, z_t) = (-5, 27, -30)mm$
- Tumor 3 $(x_t, y_t, z_t) = (-25, -20, -30)mm$

After viewing figure 11, we can conclude that in the absence of the calibration, the energy does not focus and, therefore, the tumor is not detected. Furthermore, the tumor can be detected using Ideal Calibration and doesn't present any clutter. In addition, with the figure 11b, we can conclude that the tumor can be detected with SVD calibration, but has much clutter spread in the image, making tumor detection difficult.

Regarding Tumor 2, it is possible to conclude that although the tumor is detectable using the ideal calibration method, which is totally normal, the tumor is not detected with the SVD calibration method, mainly due to the fact of the algorithm be affected by the non-symmetric distance between the antennas and the breast surface due to the breast being elliptical and also large.

Finally, regarding the analysis of the results of the images obtained through the reflection coefficients for Tumor 3, we
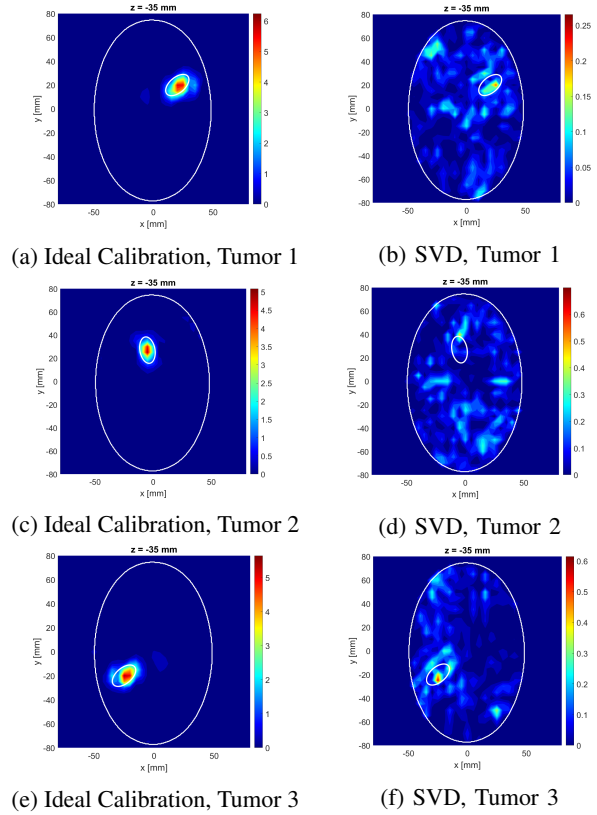

(a) Ideal Calibration, Tumor 1   (b) SVD, Tumor 1

(c) Ideal Calibration, Tumor 2   (d) SVD, Tumor 2

(e) Ideal Calibration, Tumor 3   (f) SVD, Tumor 3

Fig. 11: Imaging results for the plane z=-35mm considering the three tumors, all XETS antennas and using the ideal calibration and the SVD. The white lines translate the border of the breast with the air and the border between the tumor and the fat.

can conclude that the tumor can be detected with Ideal Calibration and the position correspond the real position, without any deviation. Furthermore, the Tumor 3 can be also detected with the SVD algorithm, as it can be seen in figure 11d.

B. IT's Breast Scanning Setup

1) Setup Description: The Antennas and Propagation group at Instituto de Telecomunicações (IT) built a contactless microwave imaging system, that is a dry setup.[21], [22] The setup is divided into two parts: Hardware and Communication. In order to summarize all the components involved in the IT imaging setup and the relationships between them, a block diagram was developed, which can be seen in figure 12.

The hardware of the set-up can be divided in three different types of components according to the role that the components have in the set-up, this is, set-up control, radio-frequency measurements and body simulation components. The set-up structure consists of a plexyglass table in order to be transparent, allowing to see the set-up. In the examination, the patient would be in prone position with the breast inside the hole.

The set-up control components are responsible for controlling the movements of the antenna's ring and the camera. A Raspberry Pi0 is programmed to control the camera and the motor and it is powered by the power bank. During
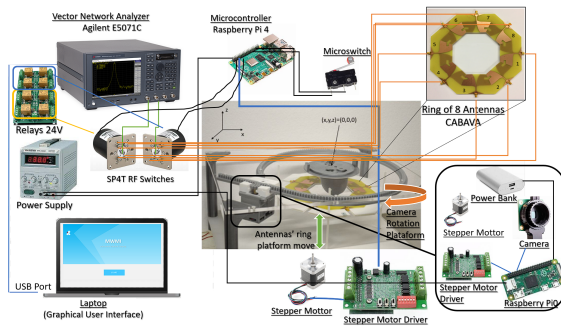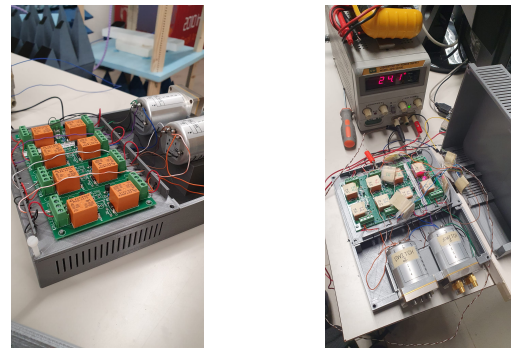
Fig. 12: Block diagram of the IT imaging system.

(a)   (b)

Fig. 13: Images captured in the lab to show the two switches connected to the relays and these being powered by a 24V voltage generator.8 SPTD channel relay and two coaxial RF Selector Switches.

the examination, the camera takes multiple snapshots of the phantom, from different positions. The information contained in the pictures is used to build the breast mask. There are two motors, where the first is characterized for an unidirectional communication with the Raspberry Pi 0. The technician gives a certain amount of time and the motor makes the cart move, along the rails. The second motor controls bearing, which make the antennas' ring platform move upwards and downwards.[22] The setup required the incorporation of 2 micro-switches, that is limit switch. One was installed top the ring of the antennas in order to stop its movement and the other micro-switch was incorporated to stop and change the direction of the camera movement. The micro-switches are connected to the Raspberry Pi 4, the same that is used by the switches to get the scattering parameters.

The radio-frequency components have the objective to radiate waves and measure the S-parameters. The ring is around the breast, in a circular way, and has 8 Circular Array Balanced Antipodal Vivaldi Antenna(CABAVA). The ring can go upwards and downwards, and that's why it is possible to take several scans of the breast, at different heights. A 4-port VNA E5071C series is used as signal source and receiver to perform the measurements of the reflection and transmission coefficients. The VNA is calibrated with an ECal module. After the calibration, the antennas are connected to the VNA with coaxial cables. As the set-up has 8 antennas and the VNA only has 4 ports, it is not possible to connect all the antennas to the VNA at the same time. Therefore, during this work, it was incorporated two switches to have up to eight antennas connected. In addition, a 8 Single Pole Double Throw(SPDT) channel relay board with a power supply of 24 Volt is used, made up of 8 channels, thus allowing to connect to two switches and is used because it is necessary to control the circuit when we select the antennas that we want to measure and get the scattering information. The two switches are controlled by a Raspberry Pi 4 and are activated using a voltage generator to feed them. The Figure 13 represents the connection between the two switches with the relays.

Finally, the body simulation components are the components used to test the microwave imaging technique and they mimic the properties of the human body, such as the electric properties and light scattering. The phantom has an anthropomorphic container and the container was made with PLA, which is a material that has a lower permittivity when it is compared with the breast skin.

IT's Breast Scanning Setup is based on a radar-based MWI and this method approaches the difference between dielectric properties of malignant and surrounding tissues. The electrical properties of tissues exhibit strong dependence on frequency (frequency dispersion) in the RF and microwave bands and it is dictated by the significant amount of water in living tissue.

The phantom built to take the measurements belongs to the group, where the adipose tissue content varies between 85% and 100%. In order to simulate the tissues' dielectric properties, the liquid Triton-X 100 is the best option and there is no need to dilute Triton-X 100 (concentration is 100%). The liquid, that simulates the properties of the tumor and the fibroglandular tissues, consists on a mixture between Triton-X 100 and salted water, where the fibroglandular tissues have a mixture with a Triton-X 100 concentration of 25% and the tumor has a mixture with a Triton-X 100 concentration of 20%.

The communication of the setup is responsible to control all hardware devices and components via PC, in order to automate the setup. The first way corresponds to the VNA being connected to the PC via USB, in such way that the compatibility with the software code can be assured. The other distinct ways consists of the PC generating a Wi-Fi network and each of the Raspberry Pi of the set-up connecting to the PC using their own IP addresses.

2) Graphical User Interface (GUI): The Graphical User Interface (GUI) is a user-friendly interface created using MATLAB software, whose main purposes are to simplify equipment handling and calibration by the user and make all the measurement procedure less time consuming. The application was developed during the works [21] and [22]. The Graphical User Interface is divided in three main menus, which are Setup, Calibration and Exam. While the menus designed for the technician are the Setup and Calibration menus, the menu designed for the doctor is only the Exam menu.

The Setup menu is composed by multiple sub-menus related withe equipment that will be used during the exam, which includes configuring the VNA, the wiring network and even

the Raspberry Pi.

The Calibration menu calculates the distance introduced by the CABAVA antenna and also obtains the free space measurements. The coefficients of free space are important in the application of the SVD method.

The main function of the exam menu is the image reconstruction of the breast. This menu is divided in three sub-menus: Target Shape, Scanning and Imaging and it's possible to register a new patient. Target shape menu is related with the camera movement and the camera takes several snapshots of the breast, in order to construct the breast mask. The Scanning submenu controls the movement of the ring of antennas and takes the measurements of the S-parameters. Finally, the Imaging submenu display old photos and calculates the new images using the image reconstruction algorithm.

Some changes were made to the GUI, such as the introduction of buttons in each menu, as there were no buttons before. The previous procedure to change the menu was if the mouse was in a predefined region it was seen as a button, something that was relative if the window of the page was varied. Apart from that with the insertion of buttons and removal of loops used to change menus, the performance of the GUI has increased.

Then, the dialog box were removed as many dialog as possible and were integrated in the application's background, as can be seen, for example, in Figure 14, which depicts a configuration menu of the measurement parameters that will be sent to the VNA.
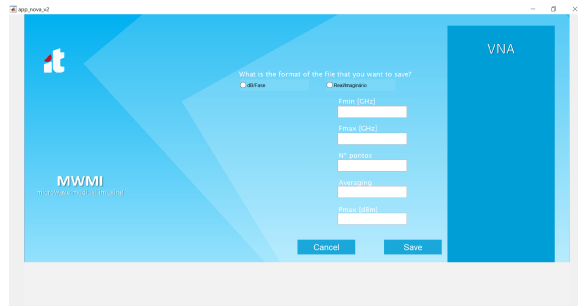

Fig. 14: VNA configuration menu.

The menus related to VNA and Raspberry Pi have now an icon to represent the status of the equipment, that is, whether it is connected or not. If the icon is red, it means that the equipment is not connected and vice versa. In figure 15, it is possible to see an example in the VNA menu.

It was added to the setup the electronic circuit, which connects the GPIO pins of the Raspberry Pi 4 to the switches and corresponds to the last step to automate the setup.

A menu, that allows selecting for each switch the antennas that will be connected and avoids conditions such as placing the same antenna on two switches, was created. The code developed in MATLAB even gives the user the opportunity to not even want to have 4 antennas connected to the 4 ports of the VNA, and can opt for less. Figure 16 represents an example where the user assumed that he only had two antennas connected to each switch, that is, antennas 3 and 1 to switch 1 and antennas 2 and 6 to switch 2, respectively.
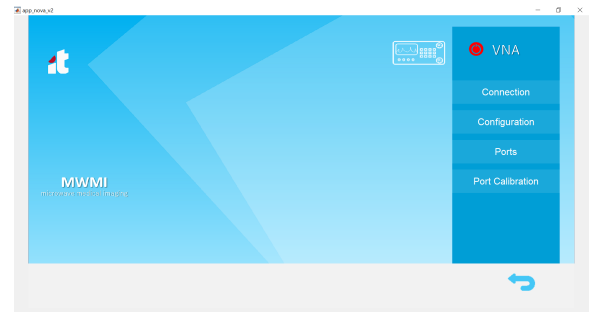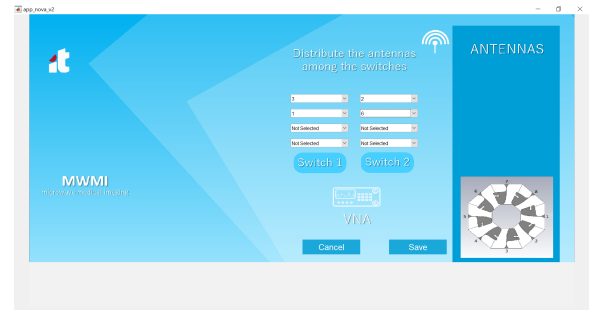

Fig. 15: VNA menu.

Fig. 16: Example with some antennas distributed by the two switches at selection antennas' menu

Furthermore, it was developed a menu that creates a table with the possible S-parameters according to the selection of antennas depending on the switches. For example, in Figure 17, it can be seen that given the selection of antennas 3 and 1 for switch 1 and 2 and 6 for switch 2, the parameters that are possible to measure are $S_{(3,3)}$, $S_{(1,1)}$, $S_{(2,2)}$, $S_{(6,6)}$, $S_{(3,1)}$, $S_{(3,2)}$, $S_{(3.6)}$, $S_{(1,2)}$ and $S_{(1,6)}$ as shown in the figure.
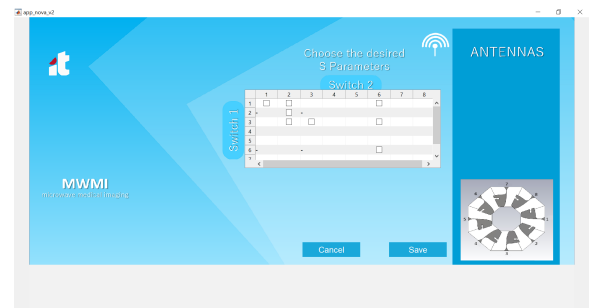

Fig. 17: Example with the S matrix considering the previous distribution of antennas.16

V. Conclusions

Microwave imaging has shown potential for breast cancer detection. In this paper, different microwave breast imaging systems are addressed. In order to gain more knowledge about this topic, some analysis and studies about image reconstruction algorithm were made.

The antenna influences the setup performance and since it is a non ideal element, the antenna introduce clutter and distortion to the measured signals. In order to overcome

obstacles like these, there is an artifact removal algorithm. The CST was used to analyze and study the behavior of the XETS antenna in relation to the target. XETS antenna provides an extremely stable phase center over the frequency band of operation and has a radiation pattern very stable with frequency, although quasi omnidirectional.

Furthermore, it was also possible to measure acquired signals with the aid of a VNA for different phantoms anthropomorphic and homogeneous. Some of the images that resulted from the reconstruction algorithm indicated the presence of clutter or the tumor was deviated from its physical position that was measured in the laboratory. In addition, the tumor was not detected using SVD in some breasts. The causes can be the breast is not symmetric, the reflection that occurs on the breast skin surface can be several orders of magnitude higher than the reflection that occurs on the tumor, et cetera.

The other part of this works regards microwave breast imaging system developed by the Antennas and Propagation group at Instituto de Telecomunicações (IT), in Lisbon. During the thesis, two switches were included in the setup, in order to obtain the reflection coefficients to which the antennas are connected, thus allowing an increase in the number of antennas to be measured during each measurement and consequently the possibility of having more S parameters in the scattering matrix. Furthermore, the Graphical User Interface (GUI) has progressed and is more developed.

References

[1] E. C. Fear and M. A. Stuchly, "Microwave breast cancer detection," in *2000 IEEE MTT-S International Microwave Symposium Digest (Cat. No.00CH37017)*, vol. 2, 2000, pp. 1037–1040 vol.2.

[2] Cancer stat facts: Female breast cancer. (April,2020). [Online]. Available: https://seer.cancer.gov/statfacts/html/breast.html

[3] B. Moloney, D. O'Loughlin, S. E. Abd, and M. Kerin, "Breast cancer detection—a synopsis of conventional modalities and the potential role of microwave imaging," *MDPI Diagnostics*, vol. 10, no. 2, 2020.

[4] D. O'Loughlin, M. O'Halloran, B. M. Moloney, M. Glavin, E. Jones, and M. A. Elahi, "Microwave breast imaging: Clinical advances and remaining challenges," *IEEE Transactions on Biomedical Engineering*, vol. 65, no. 11, pp. 2580–2590, 2018.

[5] E. C. Fear, X. Li, S. C. Hagness, and M. A. Stuchly, "Confocal microwave imaging for breast cancer detection: localization of tumors in three dimensions," *IEEE Transactions on Biomedical Engineering*, vol. 49, no. 8, pp. 812–822, 2002.

[6] R. Benny, T. Anjut, and P. Mythili, "An overview of microwave imaging for breast tumor detection," *Progess in Electromagnetics Research B*, vol. 87, pp. 61–91, 2020.

[7] Ultrasound. (April,2020). [Online]. Available: https://www.nationalbreastcancer.org/breast-ultrasound

[8] M. S. Islam, N. Kaabouch, and W. C. Hu, "A survey of medical imaging techniques used for breast cancer detection," in *IEEE International Conference on Electro-Information Technology , EIT 2013*, 2013, pp. 1–5.

[9] S. Kwon and S. Lee, "Recent advances in microwave imaging for breast cancer detection," *International journal of biomedical imaging*, vol. 2016, p. 5054912, 2016. [Online]. Available: https://europepmc.org/articles/PMC5210177

[10] Y. Kuwahara, S. Miura, Y. Nishina, K. Mukumoto, H. Ogura, and H. Sakahara, "Clinical test of microwave mammography," in *2013 IEEE Antennas and Propagation Society International Symposium (APSURSI)*, 2013, pp. 2028–2029.

[11] L. Duchesne, A. Fasoula, E. Kaverine, G. Robin, and J. Bernard, "Wavelia microwave breast imaging: Identification and mitigation of possible sources of measurement uncertainty," in *2019 13th European Conference on Antennas and Propagation (EuCAP)*, 2019, pp. 1–5.

[12] L. Sani, N. Ghavami, A. Vispa, M. Paoli, G. Raspa, M. Ghavami, F. Sacchetti, E. Vannini, S. Ercolani, A. Saracini, M. Duranti, and G. Tiberi, "Novel microwave apparatus for breast lesions detection: Preliminary clinical results," *Biomedical Signal Processing and Control*, vol. 52, pp. 257 – 263, 2019. [Online]. Available: http://www.sciencedirect.com/science/article/pii/S1746809419301223

[13] S. Jeon, B. Kim, and S. Son, "Clinical trial of microwave tomography imaging," in *2016 URSI Asia-Pacific Radio Science Conference (URSI AP-RASC)*, 2016, pp. 1–2.

[14] M. Solis-Nepote, T. Reimer, and S. Pistorius, "An air-operated bistatic system for breast microwave radar imaging: Pre-clinical validation," in *2019 41st Annual International Conference of the IEEE Engineering in Medicine and Biology Society (EMBC)*, 2019, pp. 1859–1862.

[15] T. Adam Reimer, *Improving Image Reconstruction and Machine Learning Methods in Breast Microwave Sensing*. The University of Manitoba, 2020.

[16] J. M. Felício, J. M. Bioucas-Dias, J. R. Costa, and C. A. Fernandes, "Antenna design and near-field characterization for medical microwave imaging applications," *IEEE Transactions on Antennas and Propagation*, vol. 67, no. 7, pp. 4811–4824, 2019.

[17] M. R. Casu, M. Vacca, J. A. Tobon, A. Pulimeno, I. Sarwar, R. Solimene, and F. Vipiana, "A cots-based microwave imaging system for breast-cancer detection," *IEEE Transactions on Biomedical Circuits and Systems*, vol. 11, no. 4, pp. 804–814, 2017.

[18] E. Porter, J. Fakhoury, R. Oprisor, M. Coates, and M. Popović, "Improved tissue phantoms for experimental validation of microwave breast cancer detection," in *Proceedings of the Fourth European Conference on Antennas and Propagation*, 2010, pp. 1–5.

[19] A. Mashal, F. Gao, and S. C. Hagness, "Heterogeneous anthropomorphic phantoms with realistic dielectric properties for microwave breast imaging experiments," *Microwave and Optical Technology Letters*, vol. 53, p. 1896–1902, 2011.

[20] M. J. Burfeindt, T. J. Colgan, R. O. Mays, J. D. Shea, N. Behdad, B. D. Van Veen, and S. C. Hagness, "Mri-derived 3-d-printed breast phantom for microwave breast imaging validation," *IEEE Antennas and Wireless Propagation Letters*, vol. 11, no. 1, pp. 1610–1613, January 2012.

[21] C. Rebocho, *Systems for Breast Tumor Detection Using Microwave Imaging*. Instituto Superior Técnico, 2018.

[22] D. Fernandes, *Early Breast Tumor Detection Using a Microwave Imaging System*. Instituto Superior Técnico, 2019.

[23] J. Felício, J. Bioucas-Dias, J. Costa, and C. A. Fernandes, "Microwave breast imaging using a dry setup," *IEEE Transactions on Computational Imaging*, vol. 6, no. 1, pp. 167–180, January 2020.

[24] M. Lazebnik, L. McCartney, D. Popovic, C. B. Watkins, M. J. Lindstrom, J. Harter, S. Sewall, A. Magliocco, J. H. Booske, M. Okoniewski, and S. C. Hagness, "A large-scale study of the ultrawideband microwave dielectric properties of normal breast tissue obtained from reduction surgeries," *Physics in Medicine and Biology*, vol. 52, no. 10, pp. 2637–2656, Apr 2007. [Online]. Available: https://doi.org/10.1088/0031-9155/52/10/001

[25] J. M. Felício, C. A. Fernandes, and J. R. Costa, "Uwb body-implantable antenna for short range communication," in *2015 9th European Conference on Antennas and Propagation (EuCAP)*, 2015, pp. 1–3.

[26] Cst - computer simulation technology. (July,2021). [Online]. Available: https://www.cst.com/

[27] J.Felício, C.Fernandes, and J.Costa, "Microwave imaging using the kirchoff migration algorithm," *Instituto de Telecomunicações*, 2015.

[28] R. A. Martins, J. M. Felício, J. R. Costa, and C. A. Fernandes, "Comparison of slot-based and vivaldi antennas for breast tumor detection using machine learning and microwave imaging algorithms," in *2021 15th European Conference on Antennas and Propagation (EuCAP)*, 2021, pp. 1–5.

[29] N. Joachimowicz, C. Conessa, T. Henriksson, and B. Duchêne, "Breast phantoms for microwave imaging," *IEEE Antennas and Wireless Propagation Letters*, vol. 13, pp. 1333–1336, 2014.